9-2-2005

Low-Voltage Ionization of Air with Carbon-Based Materials

M. S. Peterson

W. Zhang

T. S. Fisher

S V. Garimella
Purdue University, sureshg@purdue.edu

Peterson, M. S.; Zhang, W.; Fisher, T. S.; and Garimella, S V., "Low-Voltage Ionization of Air with Carbon-Based Materials" (2005). *CTRC Research Publications*. Paper 19.
http://dx.doi.org/10.1088/0963-0252/14/1/

Low-voltage ionization of air with carbon-based materials *

M.S. Peterson, W. Zhang, T.S. Fisher†, S.V. Garimella

School of Mechanical Engineering, and Birck Nanotechnology Center

Purdue University

West Lafayette, Indiana 47907

July 10, 2005

Abstract

Polycrystalline diamond and carbon nanotubes exhibit excellent vacuum field emission properties, characterized by low turn-on voltage and high current density. Their atmospheric field emission and ionization capabilities are reported in this paper. Highly graphitic polycrystalline diamond (HGPD) film was grown in a plasma-enhanced chemical vapor deposition process, and its ability to ionize atmospheric air was characterized and compared against carbon nanotubes. The HGPD sample was activated by applying a moderate voltage bias (340V) for an extended period across a 10 μm electrode gap. After activation, a turn-on voltage of 20 V and a sustainable current of 10 μA was observed with the same gap. Results also indicate that field emission helps to create a moderate ionization effect without catastrophic air breakdown. A hydrogen plasma treatment is shown to restore emission current back to or even exceeding the original level, which suggests an important role of surface termination in electron emission process. Carbon nanotubes were grown and tested but did not perform as well under similar conditions.

*Paper submitted to the *Plasma Sources Science and Technology*

†Please address all correspondence to tsfisher@purdue.edu

INTRODUCTION

The negative electron affinity (NEA) [1] and grain-boundary geometric field enhancement of polycrystalline diamond make this material an ideal low-voltage electron field emission source. In addition to its excellent field emission properties, the integrity and longevity of diamond are beneficial for practical devices operating either under vacuum or at atmospheric pressure. Particularly in ion generation devices, ion bombardment of the cathode surface requires the cathode material to possess superior mechanical strength and chemical inertness. Traditional ion generation devices suffer from inherent difficulties of operation at high voltages; therefore they are very difficult to integrate into low-voltage microscale ion-generation devices, which have potential applications in microscale mass spectroscopy [2], ion mobility spectroscopy [3], and microscale electronics cooling devices [4]. A microscale ionization device equipped with low-voltage field emission cathode is likely to become a potential efficient ion source.

In addition to polycrystalline diamond, carbon nanotubes (CNTs) exhibit excellent potential as low-voltage cold electron sources [5]. CNTs can enhance macroscopic electric fields by several orders of magnitude as a result of their high aspect ratios. Zhao and Buldum [6] used density functional theory (DFT) to show that field emission from CNTs is enhanced by the absorption of various gas molecules (O_2, N_2, etc.), suggesting an ion generation device utilizing carbon nanotubes. One concern when utilizing CNTs for producing ions is their long-term robustness as field emitters. Bonard et al. [7] reviewed CNT degradation mechanisms and showed that degradation is often caused by mechanical failure of the contact at low applied fields, and by resistive heating (probably exacerbated by mechanical stress) at high emission currents. This paper describes the synthesis and performance of highly graphitic polycrystalline diamond (HGPD) films and CNTs used as low-voltage atmospheric ionization sources.

The key processes in vacuum field emission from diamond are the injection of electrons into the conduction band and the transport of electrons to the surface from which they are emitted into vacuum by quantum tunnelling [8]. However, the detailed emission mechanism of NEA diamond films is not as well understood as that of other carbon-based materials such as carbon nanotubes [9]. De-

sirable features in a diamond field emitter typically include low resistivity, high defect density and high grain boundary density [10]. These desired properties can be achieved by depositing diamond films with high graphitic content (making the film conducting), doping (introducing inter-band energy levels and adding defects), and nanocrystalline forms of diamond (increasing grain boundary density).

In atmospheric environments, field-emitted electrons collide with neutral air molecules and ionize them with some probability. The impact ionization probability is determined by the electron energy and the associated electron-molecule cross-sections. A released electron can also ionize air molecules once its kinetic energy exceeds a threshold ($\sim$ 15 eV in air), resulting in an avalanche process. The number of ionizing collisions undergone by an electron per unit length in the direction of an electric field is referred to as Townsend's first ionization coefficient, α [11]. The combined field emission and air ionization process can produce a self-sustained current flow (ranging from picoamperes to microamperes) between an anode and a cathode without catastrophic breakdown. Zhang et al. [12] simulated the dominant collision reactions with a direct simulation Monte Carlo technique and predicted ion generation rates in atmospheric air due to field-emitted electrons. Their results indicated that undestanding the role field-emitted electrons is pivotal to better understand ionization in electrode spacings ranging from 1 to 10 μm.

Paschen [13] studied the relationship between the breakdown voltage of a gas and the product of pressure, p, and gap separation, d. The resulting Paschen's curve represents breakdown voltage as a function of pd. At very low and very high values of pd, deviations from Paschen's curve become evident , and Paschen's curve is no longer valid. The breakdown curve in microscale gaps has been investigated more recently by Torres and Dhariwal [14], who reported significant deviations from Paschen's curve at gap separations between 0.5 and 25 μm for several different cathode materials. Dhariwal et al. [15] later provided an explanation for the deviation based on tunnelling of electrons in a study of micro-motors and micro-actuators. Lee et al. [16] observed results similar to those of Torres and Dhariwal while investigating electrode erosion caused by arc discharges. Slade and Taylor [17] compared the work of Dhariwal et al. and Lee et al., and applied a linear-fit equation

to the breakdown voltage versus gap spacing data. They also introduced the effect of cathode micro-projections into the Fowler-Nordheim equation to quantify the role of field emission as a major electron source in the breakdown process. Despite the cited works, the ionization process in microscale gap with carbon-based field emission cathode has not been well tested and documented.

To investigate the generation of ions in air, it is necessary to understand both field emission and subsequent electron-air molecule impact ionization processes. Most prior work has focused on electron emission in vacuum; however, more recent studies have suggested that the presence of environmental gases can enhance field emission [19, 20, 21, 22, 23]. Field emission from polycrystalline diamond exhibits significantly higher emission current density and lower turn-on fields when compared to, for example, tungsten emitters. Diamond is also well-known to be the hardest chemically-inert material, and thus is expected to survive ion bombardment. Nanoscale structures made of polycrystalline diamond can be fabricated and used to enhance macroscopic electric fields. Kang et al. [24] fabricated molded polycrystalline diamond tips using conventional silicon microfabrication methods in conjunction with diamond deposited by plasma-enhanced chemical vapor deposition. They achieved a radius of curvature at the tip of the samples between 5 and 10 nm. The small radius of curvature increases the local electric field at the tip by geometrically enhancing the applied macroscopic electric field. Carbon nanotubes also enhance macroscopic electric fields due to their high aspect ratios, but their applicability and long-term reliability for ionization of air remains questionable. As air molecules are ionized, positive ions impact the cathode surface at relatively high energies, typically forcing an electron to be released from the cathode surface. This process can degrade the performance of the emitting surface over a period of time. Highly graphitic polycrystalline diamond and CNTs emitters are grown and compared as low-voltage atmospheric ion generators in this work. The overall goal of this paper is to investigate the emission and ionization properties of carbon-based cathode in atmospheric air.

Sample Preparation and Experimental Setup

Carbon nanotube (CNT) and highly graphitic polycrystalline diamond (HGPD) sample synthesis occurred in a SEKI AX5200s microwave plasma-enhanced chemical vapor deposition reactor. Synthesis parameters for CNT and HGPD samples, such as substrate voltage bias (DC), microwave plasma power, chamber pressure, and process gas (H_2 and CH_4) flow rates, are listed in Table I. For HGPD, a diamond-powder-scratched tungsten substrate was prepared, and for CNTs, a 20-nm aluminum and a 4-nm iron catalyst layer were thermally evaporated on a silicon substrate.

For the HGPD film, the pre-polished tungsten substrate was placed on a 5.10 cm diameter molybdenum puck and inserted into the reactor chamber. The puck served to concentrate plasma directly above the sample. The chamber was slowly evacuated to a pressure of 133.3 Pa (1 torr) by an external mechanical pump. Hydrogen (Praxair 4.5 grade) gas was then introduced into the chamber maintained at approximately 799.9 Pa (6 torr) for ten minutes at a flow rate of 50 sccm (standard cubic centimeters per minute) to purge the chamber. The chamber was then pressurized with hydrogen gas to 5333 Pa (40 torr) at a flow rate of 200 sccm. Induction substrate heating was applied by a 3.5 kW RF source acting on a graphite susceptor upon which the molybdenum puck rested. A K-type thermocouple embedded in the center of the susceptor and located at a depth of 2.54 mm from the top of the susceptor surface allowed feedback control. The temperature of the substrate's top surface was measured by a Williamson (model 90) dual wavelength pyrometer focused on top of the substrate. After the susceptor temperature stabilized at 630 ^{o}C (the pyrometer reads 770 ^{o}C for the sample surface temperature), a hydrogen plasma was initiated at a power of 1000 W. The plasma was maintained by a 2.45 GHz microwave generator (ASTeX AX2100). A -200 V bias was applied to the substrate, followed by initial methane (Praxair ultra high purity) introduction at a flow rate of 8 sccm, beginning the one-hour nucleation process. At the end of the nucleation process, substrate bias was reduced to -100 V, and the methane flow rate was reduced to 4 sccm to begin the 12-hour growth process for the diamond film. After terminating diamond synthesis, the reactor was evacuated, and the sample was allowed to cool to room temperature. Nitrogen gas (Praxair 4.8 grade) was then introduced to pressurize the chamber, and the sample was removed. CNT growth was performed in the same manner with different synthesis parameters

in which growth typically lasted 15 to 30 minutes without the nucleation step and with a plasma power of 150 W.

After growth of each sample, scanning electron microscope (SEM) images were recorded. A continuous HGPD film can be observed in Fig. 1(a) with a grain size of approximately 1 μm. Figure 1(b) shows the edge of the HGPD film and the exposed tungsten surface. The thickness of HGPD film is estimated to be approximately 3 μm. Figure 2 shows the mat-type, highly-packed multi-walled CNT array sample with approximately 40 nm diameters and 1 μm length, typical of CNTs synthesized by PECVD [25]. A Raman spectrum of HGPD was recorded and is shown in Fig. 3. The peak at 1335 cm^{-1} is a clear indication of diamond (sp^3) bonding while the peak at 1580 cm^{-1} reveals the substantial presence of graphitic (sp^2) carbon content in the sample.

The major elements of the point-to-plane two-terminal apparatus, shown in Fig. 4, are two electrodes: an anode and a cathode. The anode refers to the positively biased electrode, whereas the cathode refers to the negatively biased electrode. Most experiments were conducted in the forward bias mode with the emitter sample as the cathode and a silver rod as the anode while some samples were tested under reverse bias. Air was ionized by physically separating the anode and cathode by a controlled distance and then applying a voltage bias between the electrodes. Typical operating voltages were on the order of several hundreds of volts, and the measured currents ranged from fractions of picoamperes to tens of microamperes. Current measurements were obtained from a Keithley 6485 picoammeter via an IEEE-488 (GPIB) bus connected to a PCI-GPIB controller installed on a personal computer. Current-voltage results presented in this paper represent the average current from 200 data samples per applied voltage that were recorded over an 11.5-second period with a 0.058 s interval between readings. Voltage measurements were obtained from a KEPCO BHK power supply and represent the local voltage at the output terminals. An inchworm motor, which utilizes piezoelectric actuators attached to a linear translation stage with crossed-roller bearings, was used to control the spacing between anode and cathode. An optical position encoder and feedback loop were incorporated into the inchworm motor to provide 0.5 μm spatial resolution. The 75 mm $\times$ 75 mm translational stage was mounted directly to an optical tabletop.

A micromanipulator was also attached to the translation stage and held the 3 mm diameter silver rod anode. The sample was sandwiched between a 7.0 mm thick Plexiglas plate with approximately 25 mm diameter through-holes to accommodate various sized samples and a molybdenum electrical contact plate, which was placed on top of a 6.0 mm thick plate of glass (as shown in Fig. 4). A Plexiglas container enclosed this entire apparatus to prevent dust and any room drafts from affecting the experiment.

Results and Discussion

The HGPD sample was tested on the two-terminal apparatus described in the previous section. In the first test, a current of 10 nA was measured at 300 V forward bias with a 10 μm gap separation. The voltage was then increased to 340 V and held constant for approximately 12 hours. Application of the constant voltage for an extended period of time produced improved emission results [26]. Current as a function of time in the initial 12-hour activation process is shown in Fig. 5. The initial current of tens of nanoamperes increases sporadically and finally increases to several microamperes. After the activation process, current-voltage tests were performed and the results are shown in Fig. 6. The inset of Fig. 6 shows the low current range. It can be seen that the sample turned on at approximately 20 V after the initial activation process. The turn-on voltage is defined as the voltage needed to maintain a 5 pA current, which is slightly above our average circuit noise level. Above-turn-on voltages generated several microamperes of current subsequently. A maximum current of 10.4 μA was recorded at 340 V, which was the maximum voltage applied during this test.

The same location on the sample was then tested at 340 V for long-term reliability and resulted in a second activation process. Figure 7 shows a current versus time plot over a 40-hour time period. Significant current fluctuation in the first 15 hours is observed. After the first 15 hours, the current increased rapidly and remained relatively stable at approximately 10 μA for 25 hours. Current-voltage tests were performed again after the 40 hour activation test (see Fig. 8). The inset of Fig. 8 shows that the sample turned on at approximately 20 V for both gap separations. For the 10 μm gap, the current increased rapidly up to an applied voltage bias of 100 V, where it plateaued

at approximately 5 μA up to 200 V. Increasing the voltage beyond 200 V caused the current to continue to increase until the test was stopped at 250 V. At a gap separation of 20 μm, the sample turned on at 20 V, and the current continued to increase gradually as the voltage was increased to 250 V. For this 20 μm gap test, current levels were approximately one order of magnitude less than those at the gap separation of 10 μm over most of the voltage range.

After activating a second spot on the sample for several hours at 240 V, several current-voltage tests were performed at a series of different gap separations (2, 3, 4, 5, 6, 8, 10, and 12 μm), and turn-on voltages are shown in Fig. 9 compared to the traditional Paschen's curve on iron cathode surface [27] and the electrical breakdown voltage curve [16]. The turn-on fields for the respective gap separations were as follows: 35, 33, 30, 32, 28, 25, 21, and 22.5 V/μm, which are significantly larger than the results on the first spot, indicating the non-uniformity of the HGPD film. The turn-on field generally decreases as the air gap increases because more ionization events occur and release free electrons inside the gap, thus generating larger currents as the gap increases. For very small gaps (significantly less than the mean free path of electrons in air), negligible numbers of molecules are ionized along the nearly ballistic electron path, and the current measured is primarily caused by field emission alone. Between gaps of 2 and 12 μm, the current likely derives from a combination of ions and electrons produced by impact ionization and field emission. As the gap becomes larger, the voltage needed to create the same magnitude of electric field must increase and quickly approaches the breakdown voltage, meaning that catastrophic breakdown would occur before significant field emission is initiated. Therefore, the region between Paschen's curve and the turn-on voltage curve in Fig. 9 is the working area for micro-scale field-emission ionization devices.

After several days of testing, the emission current from the sample degraded to a few nA at 300 V applied voltage and 10 μm spacing. A hydrogen plasma regeneration process was then performed. The sample was placed back in the PECVD chamber and treated with the prior synthesis conditions without the presence of methane. Then, another long-term test with a 10 μm gap and 290 V bias was conducted on the regenerated sample, and the current as a function of time is shown in Fig. 10. The emission current reaches the 10 $\sim$ 100 μA level. We postulate that the plasma

treatment removes undesirable impurities that may have attached to the surface and replaces them with hydrogen termination, which reduces the surface electron affinity [10].

Current-voltage results in Fig. 11 correspond to the CNT sample shown in Fig. 2. Three different tests were performed on the same sample at different locations and revealed turn-on fields of 10.0 V/μm and 10.5 V/μm for the first and second forward bias tests, respectively. The sample turned-on at a slightly higher field of 12.0 V/μm for the third test under reverse bias. Maximum currents of 7.39 pA, 8.39 pA, and 3.24 pA were recorded at 200 V during ramp-up for the first, second, and third tests, respectively. In general, reverse bias tests exhibited higher turn-on fields and lower currents at equivalent voltages. It is being noted by the author that the reverse bias case has totally different underlying discharge mechanism in which field emission from diamond is not involved. The current was quite stable in the first 12 seconds period for the CNT sample as indicated by the current versus time plot in Fig. 12. The stability of the current shown in Fig. 12 confirms initial CNT-to-substrate adhesion. The testing circuit was frequently shortened for times longer than this initial period, The short circuits were likely the result of CNTs that broke away from the substrate under strong electric fields. In any case, CNTs exhibited significantly smaller currents than the HGPD under similar voltages.

Conclusions

A highly graphitic polycrystalline diamond film and CNT array were grown by plasma-enhanced chemical vapor deposition and two-terminal current-voltage experiments were performed in air under atmospheric pressure and room temperature. The results indicate that an activation process enables low turn-on voltage and sustainable microampere currents for the HGPD sample. Before the activation process, the HGPD sample exhibited relatively poor performance. After activation, it ionized atmospheric air at voltages below 350 V while providing sustainable microampere currents over a 40-hour time period. A recommended working region was identified between the breakdown curve and the turn-on voltage curve for microscale ion generation. The ionization ability of the HGPD film can be regenerated by a hydrogen plasma treatment. The tested CNT samples

show considerably smaller currents than those of HGPD under the same experimental conditions. The fact that diamond has a strongly bonded crystal structure and excellent mechanical and chemical properties makes it an attractive material for generating large quantities of ions at low voltages.

Acknowledgment

Support from the Semiconductor Research Corporation and the National Science Foundation for this work is gratefully acknowledged.

References

[1] J. Weide, Z. Zhang, P. Baumann, M.G.Wensell, J. Bernholc, and R. Nemanich, Physical Review B **50**, 5803 (1994).

[2] P. Siebert, G. Petzold, *Á.* Hellenbart, and J. Müller, Applied Physics A **67**, 155 (1998).

[3] R. Longwitz, H. Lintel, and P. Renaud, Journal of Vacuum Science & Technology B **21**, 1570 (2003).

[4] D. Schlitz, S. Garimella, and T. Fisher, in *ASME Heat Transfer/Fluids Engineering Summer Conference* (2004), 56470.

[5] J. Bonard, M. Croci, C. Klinke, F. Conus, I. Arfaoui, T. Stöckli, and A. Chatelainet, Physical Review B **67**, 085412 (2003).

[6] J. Zhao and A. Buldum, Nanotechnology **13**, 195 (2002).

[7] J. Bonard, C. Klinke, K. Dean, and B. Coll, Physical Review B **67**, 115406 (2003).

[8] O. Gröning, O.M.Küttel, P. Gröning, and L.Schlapbach, Journal of Vacuum Science & Technology B **17**, 1064 (1999).

[9] I. Krainsky and V. Asnin, Applied Physics Letters **72**, 2574 (1998).

[10] O. Gröning, L.-O. Nilsson, P. Gröning, and L.Schlapbach, Solid-State Electronics **45**, 929 (2001).

[11] E. Nasser, *Fundamentals of Gaseous Ionization and Plasma Electronics* (Wiley-Interscience, 1971).

[12] W. Zhang, T. Fisher, and S. Garimella, Journal of Applied Physics **96**, 6066 (2004).

[13] F. Paschen, Annals of Physics **37** (1889).

[14] J. Torres and R. Dhariwal, Nanotechnology **10**, 102 (1999).

[15] R. Dhariwal, J. Torres, and M. Desmulliez, IEE Proceedings- Science, Measurement and Technology **147**, 261 (2000).

[16] R. Lee, H. Chung, and Y. Chiou, IEE Proceedings- Science, Measurement and Technology **148**, 8 (2001).

[17] P. Slade and E. Taylor, IEEE Transactions on Components and Packaging Technologies **25**, 390 (2002).

[18] R. Lee, H. Chung, T. Sakashita, and K. Betsui, Journal of Vacuum Science & Technology B **19**, 912 (2001).

[19] Y. Gotoh, D. Nozaki, H. Tsuji, J. Ishikawa, T. Nakatani, T. Sakashita, and K. Betsui, Journal of Vacuum Science & Technology B **19**, 912 (2001).

[20] M. Takai, H. Morimoto, A. Hosono, and S. Kawabuchi, Journal of Vacuum Science & Technology B **16**, 799 (1998).

[21] M. Nagao, M. Matsubara, K. Inoue, Y. Gotoh, H. Tsuji, and J. Ishikawa, Japanese Journal of Applied Physics **35**, 5479 (1996).

[22] A. Driskill-Smith, D. Hasko, and H. Ahmed, Applied Physics Letters **71**, 3159 (1997).

[23] L. Pescini, A. Tilke, R. Blick, H. Lorenz, J. Kotthaus, W. Eberhardt, and D. Kern, Advanced Materials **13**, 1780 (2001).

[24] W. Kang, T. Fisher, and J. Davidson, New Diamond and Frontier Carbon Technology **11**, 129 (2001).

[25] M. Meyyappan, L. Delzeit, A. Cassell, and D. Hash, Plasma Sources Science and Technology **12**, 205 (2003).

[26] O. Küttel, O. Gröning, E. Schaller, L.Diederich, P. Gröning, and L. Schlapbach, Diamond and Related Materials **5**, 807 (1996).

[27] F. Maxfield and R. Benedict, *Theory of Gaseous Conduction and Electronics* (Mcgraw-Hill Book Company, 1941).

List of Figures

Table I: PECVD synthesis parameters for HGPD and CNT.

Synthesis parameters	HGPD	CNT
Pressure (Pa)	5333	1333
Stage Temperature (^{o}C)	630	710
Plasma Power (W)	1000	150
Bias (V)	-200 in nucleation step, -100 in growth step	0
CH_4/H_2 Flow Rate (sccm)	8/200 in nucleation step, 4/200 in growth step	9/45
Time	1 hr in nucleation step, 12 hrs in growth step	15 minutes

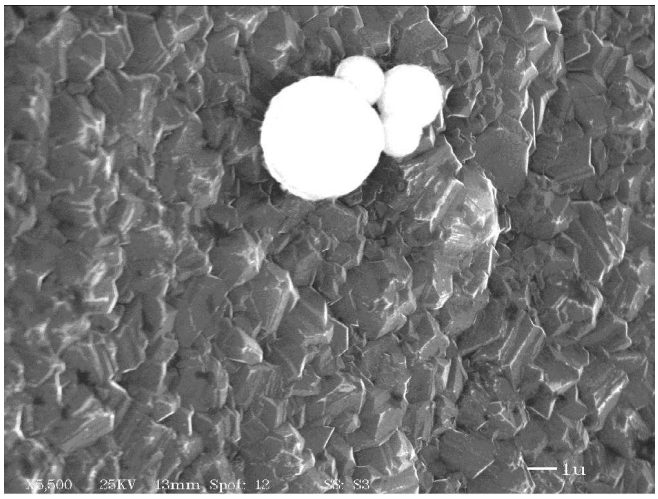

1(a): Top-view of grain and grain boundaries.

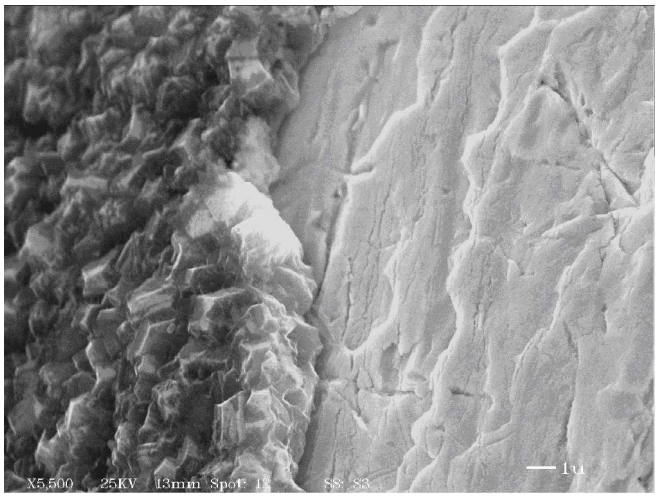

1(b): Edge-view of diamond film and exposed tungsten substrate.

Figure 1: SEM images of the highly graphitic polycrystalline diamond sample.

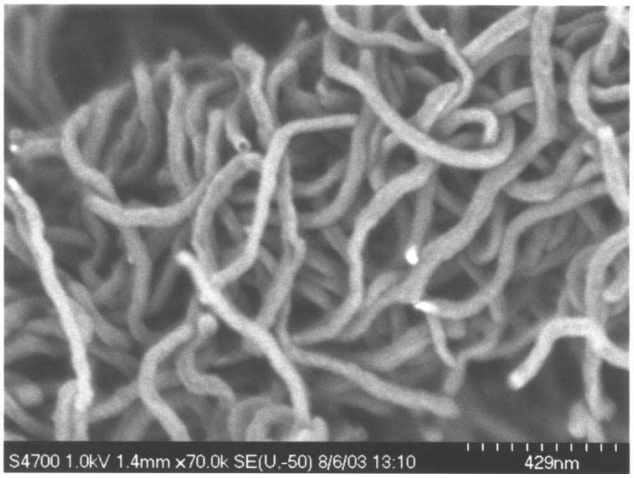

2(a): Top-view, the diameter of CNT is approximately 40 nm.

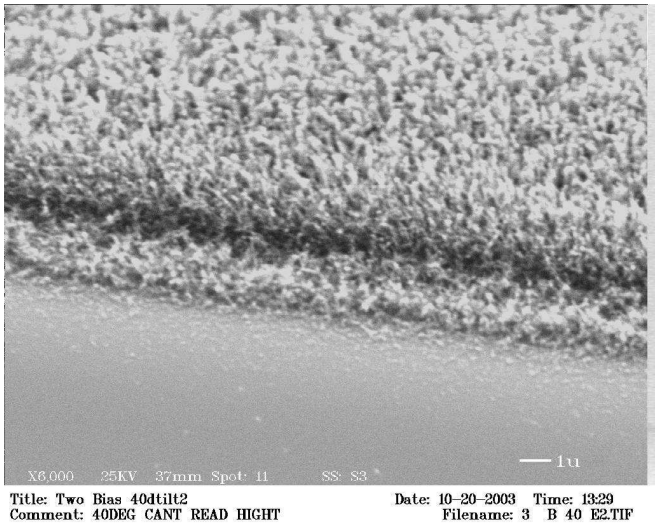

2(b): Edge-view, the length of CNT is approximately 1 μm.

Figure 2: SEM images of the CNT array.

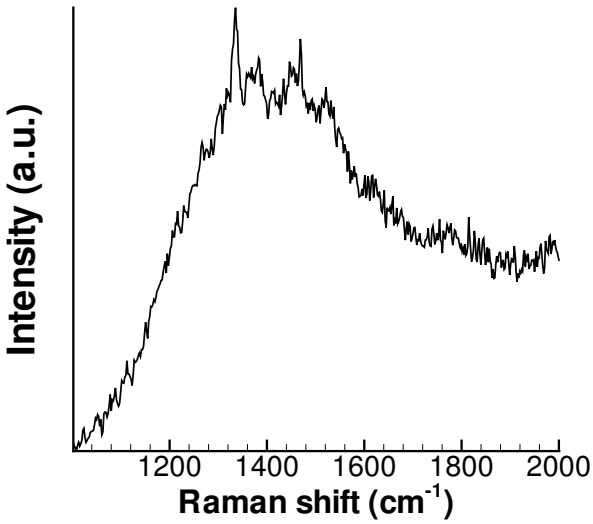

Figure 3: Raman spectrum of the highly graphitic polycrystalline diamond (HGPD) sample.

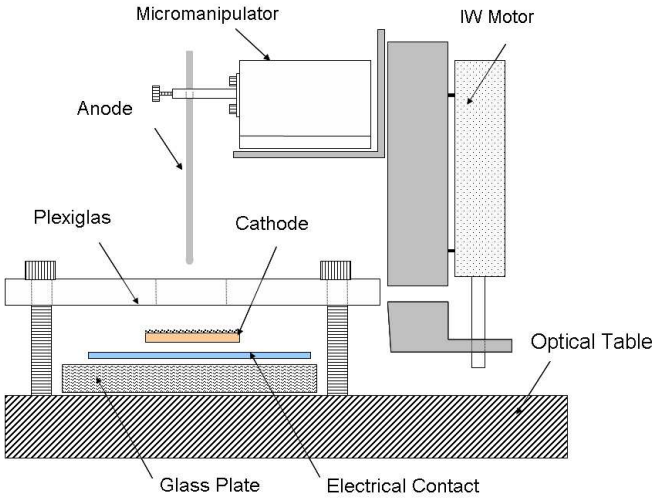

Figure 4: Schematic diagram of two-terminal point-to-plane apparatus in the forward bias setup.

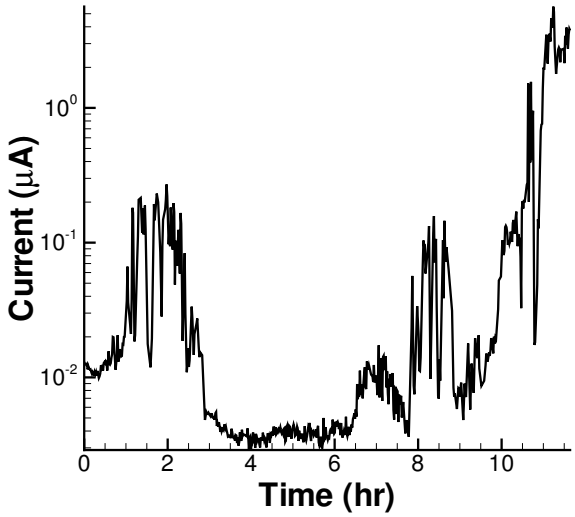

Figure 5: Current versus time plot showing initial activation of highly graphitic polycrystalline diamond sample in the first long term test. Applied bias is 340 V, test period is 12 hours.

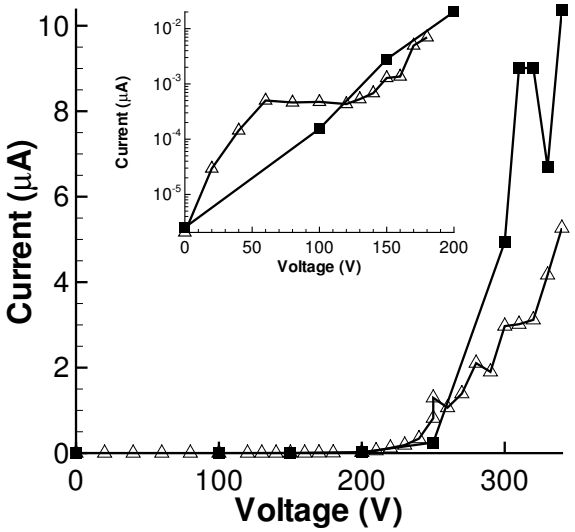

Figure 6: Current versus voltage plot after first activation process. Inset shows the same results in the low bias range. "■": ramp-up under forward bias; "△": ramp-down under forward bias.

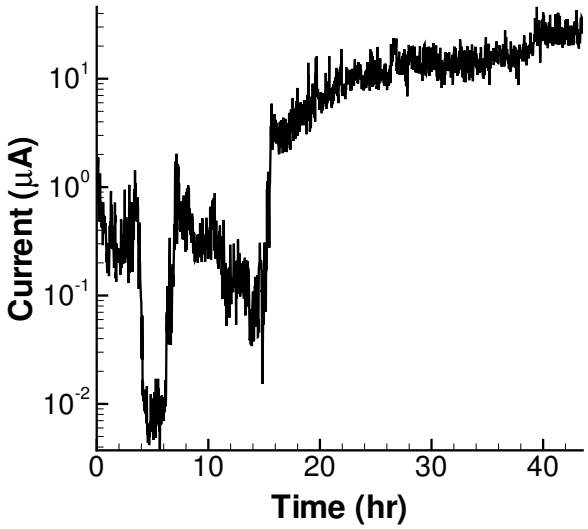

Figure 7: Current versus time plot in the second long term test. Applied bias is 340 V and test time is 40 hours.

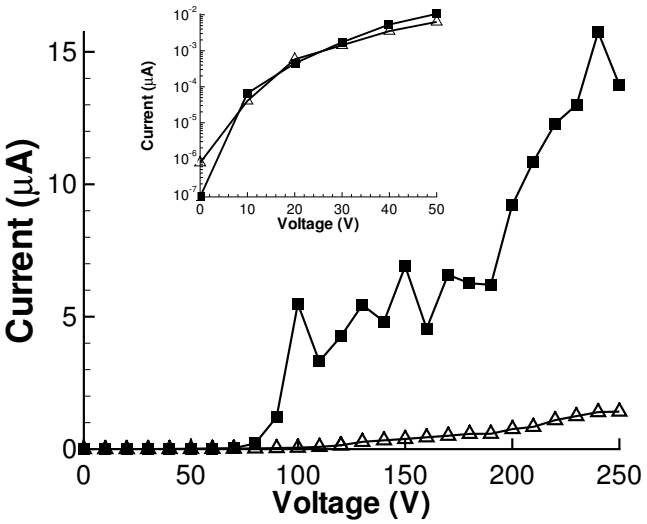

Figure 8: Current versus voltage in ramp-up under forward bias after second long-term test in 10 (■) and 20 μm (△) gaps. Inset shows the same results in the low bias range.

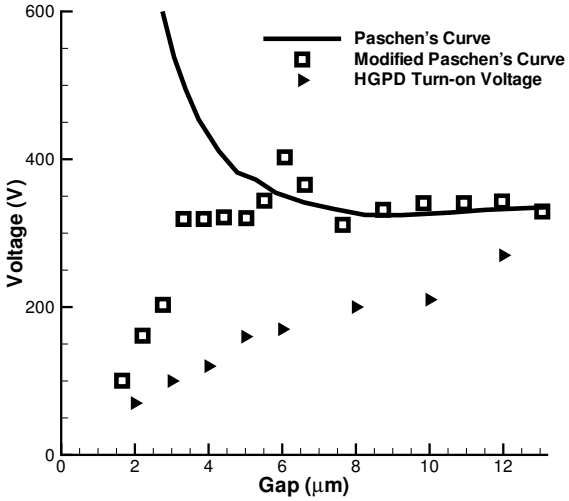

Figure 9: Comparison between traditional Paschen's curve on iron cathode surface [27], electrical breakdown voltage curve of micro-scale gap [16] and turn-on voltage curve measured in this paper. The working area of a micro-scale ionizer lies between electrical breakdown voltage curve and turn-on voltage curve.

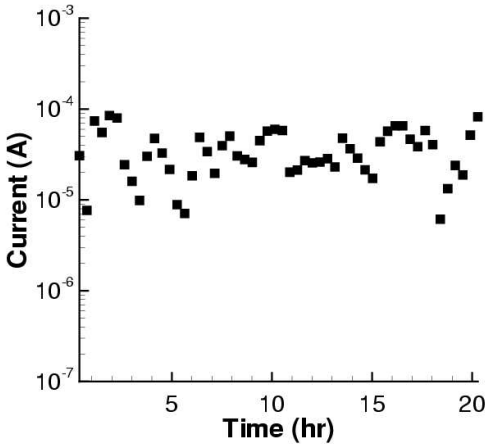

Figure 10: Current as a function of time after a hydrogen plasma regeneration treatment. The current fluctuates between 10 and 100 μA.

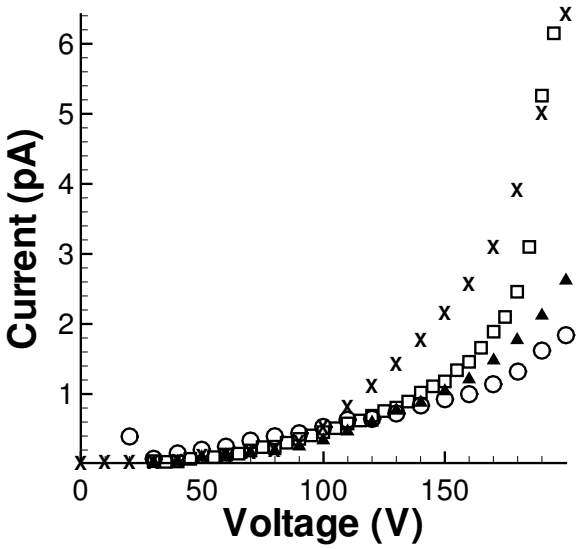

Figure 11: Current versus voltage results for three tests of mat-type 40 nm diameter multi-walled CNT array sample. "X": 1st spot ramp-up under forward bias; "□": 2nd spot ramp-up under forward bias; "■": 3rd spot ramp-up under reverse bias; "○": 3rd spot ramp-down under reverse bias.

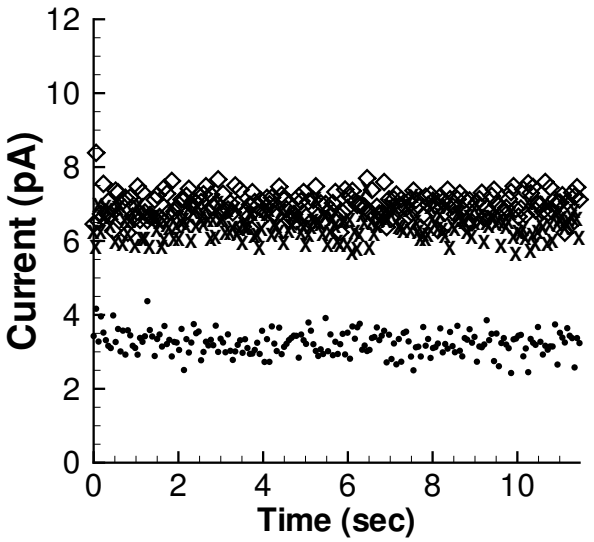

Figure 12: Current versus time for 40 nm diameter multi-walled CNT sample. "X": 1st spot; "□": 2nd spot; "■": 3rd spot.